nature

SUPPLEMENTARY INFORMATION

https://doi.org/10.1038/s41586-019-1139-x

In the format provided by the authors and unedited.

A late Middle Pleistocene Denisovan mandible from the Tibetan Plateau

Fahu Chen[1,2,15]*, Frido Welker[2,3,4,15], Chuan-Chou Shen[5,6,15], Shara E. Bailey[3,7], Inga Bergmann[3], Simon Davis[8], Huan Xia[2], Hui Wang[9,10], Roman Fischer[8], Sarah E. Freidline[3], Tsai-Luen Yu[5,6], Matthew M. Skinner[3,11], Stefanie Stelzer[3,12], Guangrong Dong[2], Qiaomei Fu[13], Guanghui Dong[2], Jian Wang[2], Dongju Zhang[2]* & Jean-Jacques Hublin[3,14]*

[1]Key Laboratory of Alpine Ecology (LAE), CAS Center for Excellence in Tibetan Plateau Earth Sciences and Institute of Tibetan Plateau Research, Chinese Academy of Sciences, Beijing, China. [2]Key Laboratory of Western China's Environmental Systems (Ministry of Education), College of Earth and Environmental Sciences, Lanzhou University, Lanzhou, China. [3]Department of Human Evolution, Max Planck Institute for Evolutionary Anthropology, Leipzig, Germany. [4]Department of Biology, University of Copenhagen, Copenhagen, Denmark. [5]High-Precision Mass Spectrometry and Environment Change Laboratory (HISPEC), Department of Geosciences, National Taiwan University, Taipei, Taiwan, China. [6]Research Center for Future Earth, National Taiwan University, Taipei, Taiwan, China. [7]Department of Anthropology, Center for the Study of Human Origins, New York University, New York, NY, USA. [8]Target Discovery Institute, University of Oxford, Oxford, UK. [9]Department of Cultural Heritage and Museology, Institute of Archaeological Science, Fudan University, Shanghai, China. [10]Gansu Provincial Institute of Cultural Relics and Archaeological Research, Lanzhou, China. [11]School of Anthropology and Conservation, University of Kent, Canterbury, UK. [12]Department of Anatomy and Biomechanics, Karl Landsteiner University of Health Sciences, Krems an der Donau, Austria. [13]Key Laboratory of Vertebrate Evolution and Human Origins, Center for Excellence in Life and Paleoenvironment, Institute of Vertebrate Paleontology and Paleoanthropology, Chinese Academy of Sciences, Beijing, China. [14]Chaire Internationale de Paléoanthropologie, Collège de France, Paris, France. [15]These authors contributed equally: Fahu Chen, Frido Welker, Chuan-Chou Shen. *e-mail: fhchen@itpcas.ac.cn; djzhang@lzu.edu.cn; hublin@eva.mpg.de

Supplementary information to:

A late Middle Pleistocene Denisovan mandible from the Tibetan Plateau

Fahu Chen[1,2]§*, Frido Welker[3,4,2]§, Chuan-Chou Shen[5,6]§, Shara E. Bailey[3,7], Inga Bergmann[3], Simon Davis[8], Huan Xia[2], Hui Wang[9,10], Roman Fischer[8], Sarah E. Freidline[3], Tsai-Luen Yu[5,6], Matthew M. Skinner[3,11], Stefanie Stelzer[3,12], Guangrong Dong[2], Qiaomei Fu[13], Guanghui Dong[2], Jian Wang[2], Dongju Zhang[2]* & Jean-Jacques Hublin[3,14]*

1 Key Laboratory of Alpine Ecology (LAE), CAS Center for Excellence in Tibetan Plateau Earth Sciences and Institute of Tibetan Plateau Research, Chinese Academy of Sciences, Beijing, CHINA.
2 Key Laboratory of Western China's Environmental Systems (Ministry of Education), College of Earth and Environmental Sciences, Lanzhou University, Lanzhou, CHINA.
3 Department of Human Evolution, Max Planck Institute for Evolutionary Anthropology, Leipzig, GERMANY.
4 Department of Biology, University of Copenhagen, Copenhagen, DENMARK.
5 High-Precision Mass Spectrometry and Environment Change Laboratory (HISPEC), Department of Geosciences, National Taiwan University, Taipei, Taiwan, CHINA.
6 Research Center for Future Earth, National Taiwan University, Taipei, Taiwan, CHINA.
7 Department of Anthropology, Center for the Study of Human Origins, New York University, New York, USA.
8 Target Discovery Institute, University of Oxford, Oxford, UNITED KINGDOM.
9 Department of Cultural Heritage and Museology, Institute of Archaeological Science, Fudan University, Shanghai, CHINA.
10 Gansu Provincial Institute of Cultural Relics and Archaeological Research, Lanzhou, CHINA.
11 School of Anthropology and Conservation, University of Kent, Canterbury, UNITED KINGDOM.
12 Department of Anatomy and Biomechanics, Karl Landsteiner University of Health Sciences, Krems an der Donau, AUSTRIA.
13 Key Laboratory of Vertebrate Evolution and Human Origins, Center for Excellence in Life and Paleoenvironment, Institute of Vertebrate Paleontology and Paleoanthropology, Chinese Academy of Sciences, Beijing, CHINA.
14 Chaire Internationale de Paléoanthropologie, Collège de France, Paris, FRANCE

§These authors contribute equally.
*Correspondence to: fhchen@itpcas.ac.cn; djzhang@lzu.edu.cn; hublin@eva.mpg.de.

Supplementary Information 1: Detailed U-Th dating

U-Th dating was performed on one bulk sample and two serial samples (SI Fig. 1) of carbonate crust adhering to the Xiahe mandible. One subsample, XH-SD-U01, 0.5 x 0.5 x 1.0 cm, was taken and gently crushed. Another relatively large segment, 2.5 x 1.5 x 1.5 cm, was also carefully separated from the mandible. Two subsamples, XH-SD-U04 and XH-SD-U06, roughly 0.2 g each, were then collected from the uppermost and lowermost portion of this segment (SI Fig. 1). After an ultrasonic cleaning step with ultrapure water, U-Th dating was applied to the three subsamples. Chemistry was conducted on class-100 laminar flow benches in a class-10,000 clean room at the High-Precision Mass Spectrometry and Environment Change Laboratory (HISPEC), Department of Geosciences, National Taiwan University[34]. After being dissolved in 7 N HNO_3 and spiked with a ^{233}U-^{236}U-^{229}Th tracer, the sample solution was added to 0.2 ml $HClO_4$ and refluxed at 90-100 ˚C overnight for over 10 hours to decompose organic material. Uranium and thorium were purified with chemical methods including Fe co-precipitation and anion-exchange chromatography[35]. After the final column separation step the separated U and Th aliquots were further treated with 0.05-0.2 ml $HClO_4$, refluxed at 90-100 ˚C for over 5 hours, and dried to effectively remove organic material and reduce polyatomic interferences. U and Th fractions were then dissolved in 1% HNO_3 (+0.05% HF) for instrumental analysis[35]. Determinations of all isotopic compositions and concentrations were made on a Thermo-Finnigan NEPTUNE multi-collector inductively coupled plasma mass spectrometer (MC-ICP-M)[35]. Half-lives of U-Th nuclides used are listed in Cheng et al. ([64]). Detailed ^{230}Th age calculation using an estimated initial atomic $^{230}Th/^{232}Th$ ratio of 4 (± 2) x 10^{-6} is described in Shen et al. ([34]). Uncertainties in the isotopic data and ^{230}Th dates are given at the two-sigma (2σ) level or two standard deviations of the mean ($2s_m$) unless otherwise noted. Together ^{230}Th dates provide a minimum age assessment of the mandible. Extended Data Table 1 contains elemental concentrations, elemental activities, and age calculations for the minimum age of the Xiahe mandible.

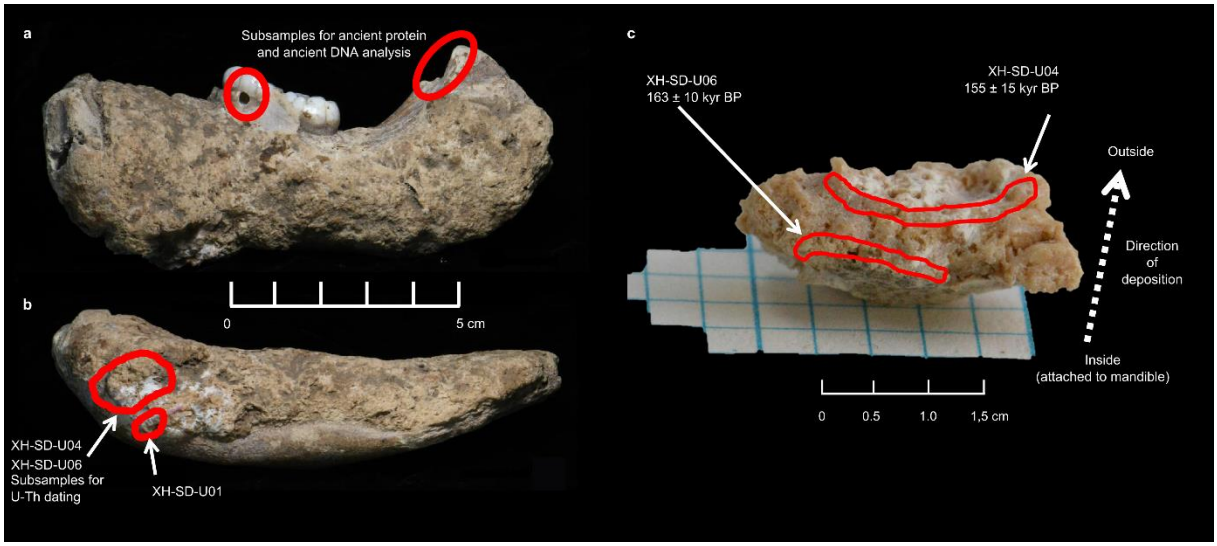

SI Figure 1. Destructive samples taken from the Xiahe mandible a, Sampling locations for ancient DNA and ancient protein analysis. **b**, Sampling locations for U-Th dating. **c**, Segment of in-situ crust carbonate from the Xiahe mandible used for serial U-Th dating.

Supplementary Information 2: Comparative samples for morphological analysis.

In the following sections, an overview of the comparative samples used for morphological analysis of the Xiahe mandible is given. In addition, several Supplementary Tables describe metrics of these comparative datasets as well as metrics taken from the (reconstructed) Xiahe mandible.

Mandibular metric data. Metric comparisons of the Xiahe reconstructed mandible with other fossil specimens were conducted with the following comparative sample (SI Table 6; references [24,67–118]). Metric details can be found in SI Table 2 and SI Figure 2. Data acquired through photogrammetric methods are equivalent in accuracy and precision to surface data generated from CT scans[119], structured-light-scans[120] and laser scans[121]. Geometric morphometrics analyses on landmark sets obtained from specimens that had been reconstructed from both conventional imaging techniques and photogrammetry revealed minor method-induced deviations that are in the range of acceptable error in osteometry[119,120]. Mean distances between meshes of CT-generated and photogrammetric scans revealed vertex displacements of 0.047 mm[119] and 0.24 mm. The latter was a result of comparing 15 (mostly fossil) mandibles that had been digitally reconstructed from both CT- and laser scans by the author (SI Table 1). The graphical display of the actual 3D-models revealed an almost complete digital overlap between methods, where anatomical traits for landmark acquisition and metric measurements were equally well expressed. The quality of 3D-photogrammetric data regarding resolution, smoothness and surface completeness is comparable to conventional techniques. The capability to capture narrow edges and holes even outperforms the laser- and structured-light technologies. Photogrammetry scans can attain resolutions of ≈260µ, which is comparable to good-quality CT scans, hence outclassing the possibilities of laser-scanning by far. Eventually, photogrammetry can successfully capture morphology of skeletal remains for any anatomical, morphometric or even taphonomic purpose[122,123]. It has been proven as reliable imaging technique for small lithic artefacts[124], detailed tooth morphology studies[125] or even entire archaeological and geological sites.

SI Table 1. Distances in mm between meshes generated from CT versus photoscans (PS). "Raw" refers to the original surface that is generated from the scan data. "Rec." means a surface where holes have been filled and edges have been reconstructed.

Specimen	Distance Raw CT ↔ Raw PS	Distance Rec. CT ↔ Rec. PS
Cro Magnon 3		0.27 mm
El Mirón 1		0.18 mm
El Sidrón 1	0.32 mm	0.31 mm
El Sidrón 2	0.19 mm	0.2 mm
Indian recent jaw	0.35 mm	0.37 mm
Kebara 2	0.12 mm	0.09 mm
La Ferrassie 1	0.26 mm	0.35 mm
La Quina 5	0.26 mm	0.34 mm
Malarnaud 1	0.17 mm	0.18 mm
Montmaurin 1	0.15 mm	0.13 mm
Pech de l'Azé		0.18 mm
Qafzeh 9	0.29 mm	
Tighenif 1	0.15 mm	
Tighenif 3	0.33 mm	0.33 mm
Zafarraya 2	0.3 mm	
Mean	**0.2408333 mm**	**0.2441667 mm**

SI Table 2. Measurements of the Xiahe mandible after reconstruction. The Xiahe mandible is compared to eight groups of fossil hominins and the Penghu mandible. Values are given in mm. $\bar{x}$ is the mean, σ is the standard deviation, n indicates sample size. () indicates that the value is an estimate. Bi-M2/Bi-M3 means Bimolar. MP means Middle Pleistocene. For measurements where only two samples are available, both are given in the relevant cell (n1 and n2).

Measurement	Xiahe	Penghu	Asian *H. erectus*	African archaic MP	European archaic MP	Asian Neanderthals	European Neanderthals	Early *H. sapiens*	Late Pleistocene *H. sapiens*	Late Pleistocene Asian *H. sapiens*
Symphyseal angle (id-gn)	**69**		**n1=60 n2=63** n=2	**$\bar{x}$ = 61.67** σ=1.53 n=3	**$\bar{x}$ = 73.33** σ=3.51 n=3	**$\bar{x}$ = 81.33** σ=3.79 n=3	**$\bar{x}$ = 72.44** σ=8.32 n=9	**$\bar{x}$ = 78.33** σ=5.69 n=3	**$\bar{x}$ = 76.50** σ=6.07 n=11	–
Symphyseal Height	**32.6**	**30.5**	**$\bar{x}$ = 37.64** σ=5.66 n=9	**$\bar{x}$ = 31.78** σ=4.10 n=6	**$\bar{x}$ = 31.0** σ=2.98 n=4	**$\bar{x}$ = 36.10** σ=3.36 n=6	**$\bar{x}$ = 33.98** σ=4.59 n=26	**$\bar{x}$ = 37.32** σ=6.33 n=9	**$\bar{x}$ = 31.87** σ=2.82 n=38	**$\bar{x}$ = 30.29** σ=4.81 n=13
Symphyseal Thickness	**15.4**		**$\bar{x}$ = 15.9** σ=3.87 n=11	**$\bar{x}$ = 17.32** σ=2.57 n=6	**$\bar{x}$ = 16.88** σ=2.06 n=4	**$\bar{x}$ = 17.2** σ=3.92 n=5	**$\bar{x}$ =15.37** σ=1.72 n=26	**$\bar{x}$ =15.56** σ=2.25 n=13	**$\bar{x}$ = 15.29** σ=2.0 n=38	**$\bar{x}$ = 13.91** σ=1.8 n=12

Corpus Height at the Mandibular Foramen	**30.7**		**$\bar{x}$ = 30.92** σ=7.93 n=13	**$\bar{x}$ = 30.80** σ=5.21 n=7	**$\bar{x}$ = 30.2** σ=2.34 n=4	**$\bar{x}$ = 33.90** σ=3.51 n=7	**$\bar{x}$ = 31.22** σ=3.64 n=43	**$\bar{x}$ = 34.90** σ=4.33 n=12	**$\bar{x}$ = 30.93** σ=3.26 n=42	**$\bar{x}$ = 30.09** σ=3.18 n=13
Corpus Breadth at the Mandibular Foramen	**17.9**	**17.8**	**$\bar{x}$ = 18.26** σ=4.30 n=13	**$\bar{x}$ = 17.96** σ=1.78 n=7	**$\bar{x}$ = 18.5** σ=2.67 n=4	**$\bar{x}$ = 17.16** σ=1.89 n=7	**$\bar{x}$ = 15.67** σ=1.56 n=43	**$\bar{x}$ = 16.28** σ=1.47 n=12	**$\bar{x}$ = 12.74** σ=1.60 n=43	**$\bar{x}$ = 13.09** σ=1.68 n=13
M1_Corp.Height	**28.7**	**27.3**	**$\bar{x}$ = 35.52** σ=10.07 n=10	**$\bar{x}$ = 32.15** σ=5.38 n=8	**$\bar{x}$ = 30.25** σ=2.21 n=4	**$\bar{x}$ = 31.65** σ=3.17 n=4	**$\bar{x}$ = 30.8** σ=3.59 n=27	**$\bar{x}$ = 33.10** σ=5.44 n=11	**$\bar{x}$ = 29.51** σ=2.19 n=29	**$\bar{x}$ = 29.11** σ=3.47 n=12
M1_Corp.Breadth	**19.6**	**20.7**	**$\bar{x}$ = 18.06** σ=3.63 n=12	**$\bar{x}$ = 18.03** σ=2.46 n=8	**$\bar{x}$ = 18.08** σ=2.76 n=4	**$\bar{x}$ = 17.54** σ=2.67 n=5	**$\bar{x}$ = 16.53** σ=1.66 n=27	**$\bar{x}$ = 17.16** σ=2.45 n=12	**$\bar{x}$ = 14.25** σ=1.57 n=26	**$\bar{x}$ = 13.54** σ=2.07 n=12
M1/M2_ Corpus Height	**26.8**		**$\bar{x}$ = 29.11** σ=3.63 n=8	**$\bar{x}$ = 31.25** σ=5.11 n=8	**$\bar{x}$ = 30.2** σ=1.65 n=4	**$\bar{x}$ = 32.40** σ=1.65 n=3	**$\bar{x}$ = 29.89** σ=3.33 n=28	**$\bar{x}$ = 33.00** σ=4.00 n=9	**$\bar{x}$ = 28.64** σ=2.30 n=33	**$\bar{x}$ = 28.63** σ=3.12 n=12
M1/M2 Corpus Breadth	**21.2**		**$\bar{x}$ = 17.80** σ=2.55 n=8	**$\bar{x}$ = 18.73** σ=3.36 n=8	**$\bar{x}$ = 18.13** σ=3.09 n=4	**$\bar{x}$ = 17.57** σ=2.25 n=3	**$\bar{x}$ = 16.33** σ=1.43 n=27	**$\bar{x}$ = 17.76** σ=2.35 n=9	**$\bar{x}$ = 14.73** σ=1.92 n=34	**$\bar{x}$ = 14.28** σ=2.71 n=12
M2_Corp.Height	**25.9**		**$\bar{x}$ = 27.37** σ=3.45 n=7	**$\bar{x}$ = 31.53** σ=5.26 n=8	**$\bar{x}$ = 29.33** σ=1.71 n=4	**$\bar{x}$ = 31.75** σ=3.82 n=6	**$\bar{x}$ = 30.09** σ=3.29 n=36	**$\bar{x}$ = 32.31** σ=4.89 n=9	**$\bar{x}$ = 27.04** σ=2.58 n=34	**$\bar{x}$ = 27.54** σ=3.35 n=12
M2_Corp.Breadth	**21.5**		**$\bar{x}$ = 17.80** σ=2.40 n=8	**$\bar{x}$ = 19.47** σ=2.52 n=8	**$\bar{x}$ = 19.05** σ=3.68 n=4	**$\bar{x}$ = 17.60** σ=1.54 n=7	**$\bar{x}$ = 16.33** σ=1.62 n=35	**$\bar{x}$ = 8.94** σ=3.08 n=9	**$\bar{x}$ = 15.02** σ=1.89 n=36	**$\bar{x}$ = 14.89** σ=2.38 n=12
Dental Arcade_Length	**55.7**		**$\bar{x}$ = 58.75** σ=5.62 n=4	**$\bar{x}$ = 62.52** σ=3.55 n=5	**$\bar{x}$ = 57.73** σ=2.55 n=3	**$\bar{x}$ = 54.78** σ=2.78 n=4	**$\bar{x}$ = 54.55** σ=3.39 n=15	**$\bar{x}$ = 59.10** σ=6.79 n=5	**$\bar{x}$ = 52.01** σ=3.49 n=27	**$\bar{x}$ = 50.85** σ=4.46 n=10
Bigonial breadth	**(96.8)**		**n1=108.6 n2=97.8** n=2	**$\bar{x}$ = 99.57** σ=13.37 n=3	**n1=98.8 n2=80.4** n=2	**$\bar{x}$ = 102.13** σ=6.22 n=4	**$\bar{x}$ = 94.16** σ=11.41 n=7	**$\bar{x}$ = 97.40** σ=14.56 n=5	**$\bar{x}$ = 99.11** σ=9.42 n=28	**$\bar{x}$ = 94.04** σ=14.81 n=11
Bicanine breadth	**42.6**		**$\bar{x}$ = 35.28** σ=2.58 n=4	**$\bar{x}$ = 34.20** 5.25 n=5	**$\bar{x}$ = 36.73** σ=1.17 n=3	**$\bar{x}$ = 36.48** σ=1.63 n=6	**$\bar{x}$ = 36.47** σ=2.41 n=18	**$\bar{x}$ = 38.08** σ=1.80 n=6	**$\bar{x}$ = 32.64** σ=2.38 n=28	**$\bar{x}$ = 31.75** σ=3.22 n=11
Bi-M2 breadth	**74.7**		**$\bar{x}$ = 65.60** σ=4.75 n=4	**$\bar{x}$ = 66.00** σ=8.67 n=5	**$\bar{x}$ = 67.13** σ=3.71 n=3	**$\bar{x}$ = 72.10** σ=1.48 n=4	**$\bar{x}$ = 68.84** σ=3.36 n=15	**$\bar{x}$ = 68.15** σ=3.25 n=6	**$\bar{x}$ = 61.75** σ=3.88 n=26	**$\bar{x}$ = 63.71** σ=3.43 n=12
Bi-M3 breadth			**$\bar{x}$ = 67.70** σ=3.37 n=3	**$\bar{x}$ = 70.74** σ=9.44 n=5	**$\bar{x}$ = 70.37** σ=3.5 n=3	**$\bar{x}$ = 74.86** σ=2.78 n=5	**$\bar{x}$ = 71.6** σ=3.18 n=15	**$\bar{x}$ = 71.80** σ=3.64 n=5	**$\bar{x}$ = 66.62** σ=4.07 n=26	**$\bar{x}$ = 68.03** σ=2.62 n=9

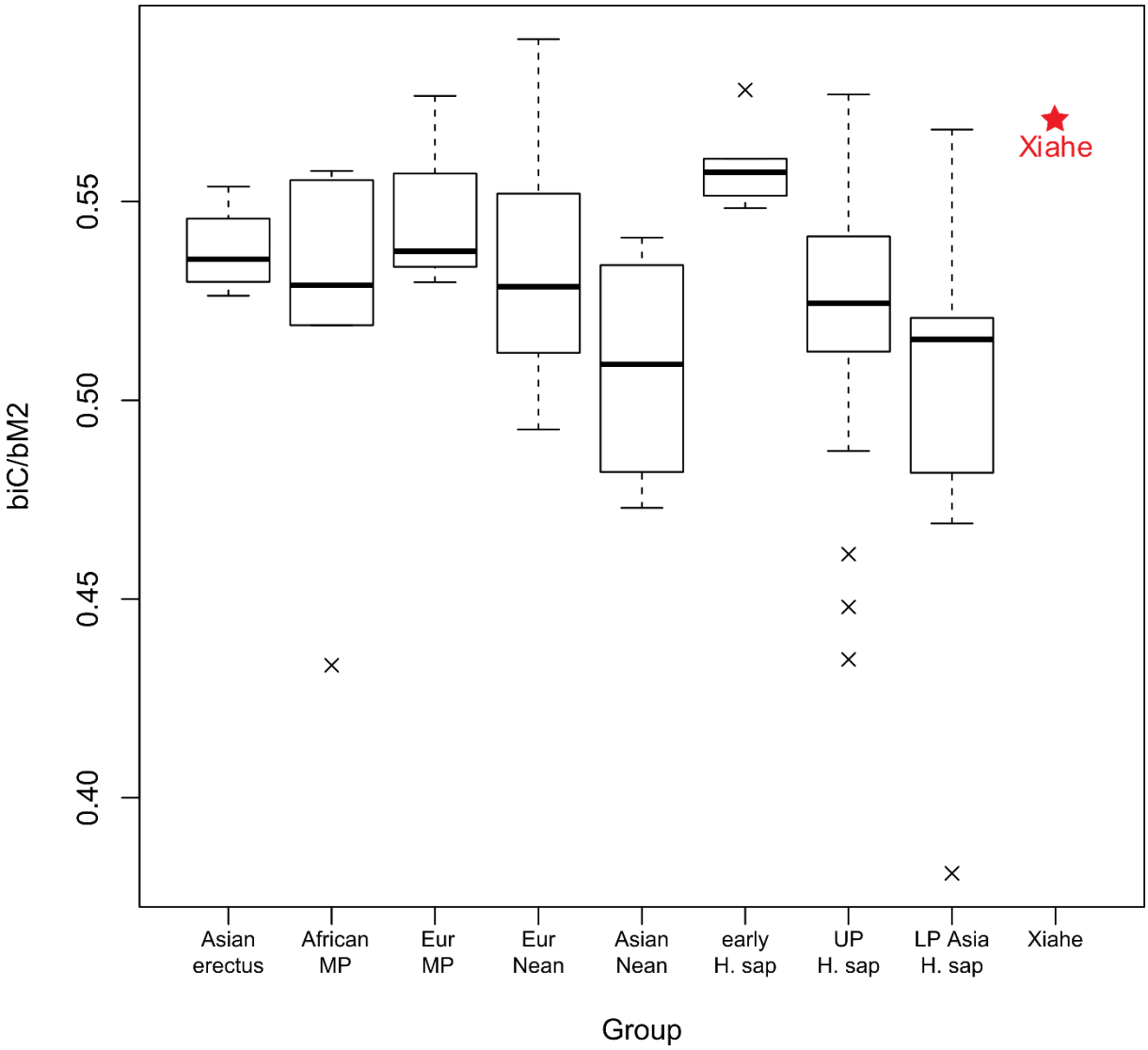

SI Figure 2. Ratio of bicanine to bimolar breadth at M2. The boxplot illustrates the median value, lower and upper quartile, minimum and maximum values and extremes. Xiahe falls at the extreme end of the comparative samples. Sample sizes: *Homo erectus* (n=4), African Middle Pleistocene (n=5), European Middle Pleistocene (n=3), European Neanderthals (n=15), Asian Neanderthals (n=4), Early *Homo sapiens* (n=6), Upper Paleolithic *Homo sapiens* (n=25), Late Pleistocene Asian *Homo sapiens* (n=11).

Shape analysis of the mandible. Geometric morphometric methods were used to analyze the shape of the Xiahe mandible in a comparative context. Comparisons were made with the specimens provided in SI Table 6. In this comparison (Extended Data Fig. 6), Xiahe plots at the edge of the *H.* erectus distribution and within the range of Middle Pleistocene *Homo*. The main shape changes along PC1 are the presence/absence of a chin and the shape of the mandibular symphysis. Like other archaic hominins (e.g., Neanderthals, MP *Homo* and *H. erectus*), Xiahe lacks a chin and its mandibular symphysis is receding, rather than vertical. Shape changes along PC2 are associated with the height of the mandibular body and length and width of the extramolar sulcus. In these features, the shape of Xiahe is similar to other Middle Pleistocene hominins, intermediate between the high corpus and long and narrow

extramolar sulcus seen in Neanderthals and *H. sapiens*, and the extremely low corpus and short and wide extramolar sulcus present in several *H. erectus* specimens.

Shape analysis of the dental arcade. In addition to geometric morphometric analysis of the mandible, a similar approach was applied to compare the dental arcade shape of the Xiahe mandible to the dental arcade shape of the specimens listed in SI Table 6.

Dental metric and non-metric data. Dental metric and non-metric data were collected directly (SI Table 6) or obtained from the literature ([25,47,126–134]). In the comparison on root number and configuration observed in the Xiahe mandible (Extended Data Fig. 8a), the three-rooted M_2 molar is of particular significance as they are very rare in non-Asian living and ancient *H. sapiens* populations, occurring in ~3% in these populations[135–137]. In those with Asian ancestry, however, the prevalence is much higher with Turner[137] finding the three-rooted M_1 in 21% - 23% of his archaeologically-derived “Eskimo” and Aleut populations.

Molar EDJ shape analysis. Analysis of molar EDJ shape was performed in reference to the specimens listed in SI Table 6. The EDJ of the M_1 exhibits a middle-trigonid crest (Bailey et al.[23]; grade 2), while on the M_2 a crest from the metaconid deflects mesially to join the marginal ridge. Cusp 7 dentine horns are present on both molars and the M_1 exhibits a fovea-type cusp 6. In addition, a principal component analysis of EDJ ridge and cervix shape (Extended Data Fig. 8b) reveals a clear separation between the *H. erectus* sample on the one hand and Neanderthals, fossil modern humans, and recent modern humans on the other. Archaic Middle Pleistocene samples sit intermediate between these groups, along with the Xiahe M_2. Morphologically this is driven by the Xiahe M_2 having a relatively shorter crown and shorter dentine horns than Neanderthals and fossil/recent humans, but a relatively taller crown and taller dentine horns than specimens of Early *Homo* and *Homo erectus*. In addition, the Xiahe M_2 differs from other Middle Pleistocene hominins in having a buccolingually expanded occlusal basin and a lingually expanded crown base.

Supplementary information 3: Dental morphology

For the detailed description of the Xiahe molars, the following abbreviations are used: protoconid (Prd), metaconid (Med), hypoconid (Hyd), entonconid (Ent), hypoconulid or Cusp 5 (Hld), tuberculum sextum (C6), tuberculum intermedium (C7), mesial marginal ridge (Mmr), interproximal wear facet (IPF), outer enamel surface (OES), enamel dentine junction (EDJ). Trait frequencies for comparative groups are provided in SI Table 3.

The M_1 crown is moderately worn with small dentine patches on the Med, Hyd, End and C7 and a larger patch on the Prd that extends towards the Mmr and Med ([138], Stage 4). There is a large mesial IPF (6.6 mm x 4.2 mm) with a branch that extends onto the occlusal margin. A small chip is missing along the occlusal-lingual boarder of the IPF. Although the M_2 is erupted and in functional occlusion, there is no distal IPF on the M1. The C7 is large (ASUDAS: grade 4) and the C6 is smaller than the Hld (ASUDAS: grade 2). At the EDJ the C6 is a single fovea-type[48]. The cusp size relationships are: Prd>Med>Hyd>End>C7>Hld>C6. The lingual face of the crown is smooth. It flares out from the cervix before turning inwards. The buccal face exhibits deep, v-shaped grooves separating the Prd/Hyd and the Hyd/Hld, which give the crown a tri-lobate appearance in occlusal view. The main buccal groove terminates in a pit. No protostylid is present at either the OES the EDJ. Enamel extension is absent. The buccal face rises more vertically than the lingual face. The trigonid is substantially higher than the talonid.

The M_2 crown exhibits facets on the End, Hyd and Hld but none on the Prd. There is no mesial IPF. There is also a small chip on the Hld on the disto-occlusal margin. The C7 is large (ASUDAS: grade 4). The cusp proportions are: Prd> Hyd>Med=End>Hld>C7. The protoconid and metaconid are separated by a deep sagittal sulcus. The M_2 is squarer and less lobate in appearance than the M1. The buccal grooves are linear rather than cleft-like. The deep buccal groove fades mid-crown and does not terminate in a pit as in the M_1. There is no protostylid present at the OES or EDJ. The C7 is bordered by distinct occlusal fissures that cross onto the lingual surface and fade about one-third the distance to the cervix. The Hyd essential ridge is bisected by a shallow fissure about mid-way to the occlusal basin.

SI Table 3. Comparative Dental metrics. Teeth are identified by letters: C, canine; M, molar; P, premolar. BL, bucco-lingual width; MD, mesiodistal length. Values are in mm. $\overline{x}$ is the mean; minimum and maximum values are between square brackets; σ is the standard deviation; *n* indicates sample size. CI: Crown index (BL/MD*100); CCA: Calculated Crown Area (BL*MD).

		Xiahe	*Homo erectus* s.l.	MP Asia	MP Africa	MP Europe	Neanderthals	Early *H. sapiens*	UP *H. sapiens*	Recent *H. sapiens*
M_1	BL	12.5	$\overline{x}$ =12.2 [10.7-13.5] σ =0.8, n = 15	--	$\overline{x}$ =11.7 [10.5-12.6] σ =0.7, n = 7	$\overline{x}$ =11.2 [11.0-11.5] σ =0.3, n = 3	$\overline{x}$ =10.9 [9.7-12.9] σ =0.7, n = 48	$\overline{x}$ =11.7 [10.5-14.3] σ = 1.0, n = 19	$\overline{x}$ =11.0 [9.2-11.9] σ =0.6, n = 42	$\overline{x}$ = 10.7 [8.6-12.6] σ = 0.7, n = 267
	MD	15.1	$\overline{x}$ =13.3 [12.1-14.9] σ =1.0, n = 13	--	$\overline{x}$ =12.8 [11.9-13.8] σ =0.7, n = 8	$\overline{x}$ =11.5 [11.3-11.9] σ =0.3, n = 3	$\overline{x}$ =11.7 [10.1-13.6] σ =0.9, n = 46	$\overline{x}$ =12.6 [10.8-14.2] σ = 1.0, n = 20	$\overline{x}$ =11.4 [10.3-12.9] σ =0.7, n = 36	$\overline{x}$ = 11.4 [9.2-13.5] σ = 0.7, n = 243
	CI	.83	.93	--	.93	.98	.94	.94	.94	.95
	CCA	188.8	157.0	--	157.0	130.5	128.0	153.1	127.0	121.1
M_2	BL	14.1	$\overline{x}$ =13.1 [11.7-14.3] σ =0.8, n = 14	$\overline{x}$ =13.0 [11.-13.9] σ =1.3 n=4	$\overline{x}$ =11.5 [10.3-12.9] σ =0.9, n = 6	$\overline{x}$ =11.2 [10.8-12.4] σ =0.6, n = 5	$\overline{x}$ =10.8 [8.6-12.4] σ =0.9, n = 44	$\overline{x}$ =11.0 [9.2-12.7] σ = 1.0, n = 22	$\overline{x}$ =10.9 [8.6-12.3] σ =0.7, n = 40	$\overline{x}$ = 10.4 [8.6-12.5] σ = 0.8, n = 207
	MD	14.5	$\overline{x}$ =13.3 [12.5-14.4] σ =0.6, n = 12	$\overline{x}$ =13.5 [12.0-14.3] σ =1.0 n=4	$\overline{x}$ =12.8 [12.0-13.8] σ =0.7, n = 6	$\overline{x}$ =12.6 [11.0-14.8] σ =1.6, n = 5	$\overline{x}$ = 11.7 [9.7-14.0] σ =1.0, n = 41	$\overline{x}$ =11.7 [10.2-14.2] σ =1.1, n = 15	$\overline{x}$ =11.3 [9.5-13.2] σ =0.8, n = 34	$\overline{x}$ = 10.9 [8.9-14.3] σ = 0.9, n = 198
	CI	.97	.97	.96	.96	.91	.93	.95	.96	.96
	CCA	204.5	153.4	190.3	145.7	147.0	125.5	139.2	123.3	111.6

SI Table 4. Comparative crown morphology. Frequencies and number of observations between brackets are provided for each feature.

	Xiahe	*H. erectus* s.l.	MP Asia	MP Africa	MP Europe	Neandert hals	Early *H. sapiens*	UP *H. sapiens*	Recent *H. sapiens*
M1 Middle Trigonid Crest [pres. >1]	absent	33.3 (12)	--	50 (2)	81.8 (5)	95.0 (40)	35.7 (14)	91.4 (35)	1.4 (207)
M1 Protostylid [pres.>1]	absent	50.0 (8)	--	33.3 (3)	0.0 (5)	0.0 (44)	12.5 (16)	5.4 (37)	0.4 (246)
M1 Cusp 6 [pres. >0]	present	28.6 (7)	--	Present (1)	0.0 (3)	38.5 (26)	0.0 (14)	17.2 (29)	18.1 (200)
M1 Cusp 7 [pres. =2-4]	present	50.0 (12)	--	0.0 (2)	0.0 (5)	22.0 (41)	42.9 (21)	5.3 (38)	9.7 (236)
M2 Middle Trigonid Crest [pres. >1]	absent	23.1 (13)	0.0 (2)	33.3 (3)	50.0 (2)	90.3 (31)	7.7 (13)	0.0 (29)	1.4 (214)
M2 Protostylid [pres.>1]	absent	20.0 (10)	Present (1)	0.0 (2)	0.0 (5)	2.8 (36)	7.1 (14)	9.1 (22)	4.6 (172)
M2 Y Groove Pattern [pres. = Y]	present	91.7 (12)	Present (1)	100 (2)	80.0 (5)	73.7 (38)	68.8 (16)	44.8 (29)	28.6 (242)
M2 Cusp 7 [pres. =2-4]	present	23.1 (13)	Present (1)	0.0 (2)	0.0 (4)	16.1 (31)	5.6 (18)	7.1 (28)	1.4 (219)
M2 Cusp 6 [pres. >0]	absent	44.4 (9)	Present (1)	--	0.0 (2)	45.8 (24)	9.1 (11)	13.3 (30)	12.7 (181)
M2 Cusp number [pres.= 4]	absent	0.0 (13)	0.0 (2)	0.0 (4)	0.0 (5)	2.4 (41)	15.8 (19)	44.0 (25)	63.8 (242)

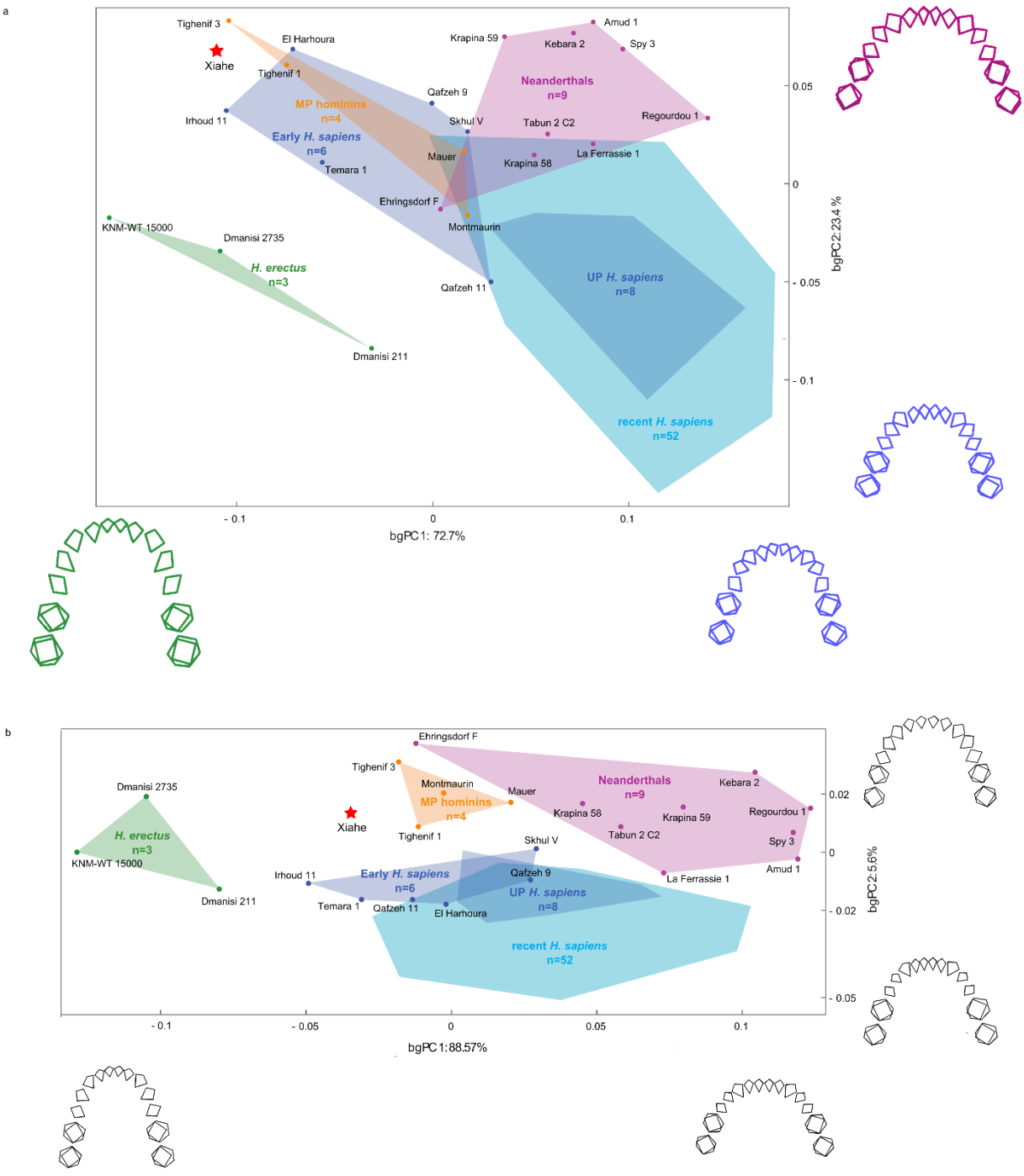

SI Figure 3. Geometric morphometrics of the dental arcade without estimated arcades. a, Procrustes form space. **b**, Procrustus shape space. For **a** and **b**, wireframes illustrate the form or shape changes along PC1 and PC2, respectively. *H. sapiens* are shown in cyan, Neanderthals in pink, *H. erectus* in green, Middle Pleistocene fossil hominins in orange, eHs in dark blue, and UPHs in light blue. Note that the position of Xiahe in relation to these fossils does not change when additional mandibular arcades are estimated based on available maxillary arcades (Extended Data Fig. 7).

Supplementary Information 4: Ancient protein analysis

The protein sequence diversity within “Denisovans” cannot be assessed conclusively as only one high-coverage genome of this hominin group is currently available (individual D3 from Denisova Cave). However, as previously demonstrated, the protein sequences from this individual, three exome-sequenced Neanderthals, and reference sequences for all great apes accurately reflect the phylogenetic relationships of these populations[9]. In addition, the Denisovan (D3) and Neanderthal proteomes derived from their high-quality genomes contain uniquely derived single amino acid polymorphisms (SAPs). The Xiahe proteome contains no spectra matching to SAPs unique to the Neanderthal or *H. sapiens* populations, however. It does contain a Denisovan-derived SAP (*COL1α2* R996K) that is not observed among any modern human sequenced as part of the 1000 Genomes project[139], or the 60,000 exomes presented by ExAc[140]. In addition, the Xiahe proteome contains a uniquely derived SAP not present in any other archaic or modern reference population (*COL2α1* E583G).
Protein sequence diversity and recovery in ancient proteomes is low compared to modern and ancient high-coverage genomes. Based on this and the absence of information on protein sequence diversity of “Denisovans”, but also taking into account the phylogenetic analysis and the occurrence of particular SAPs in various archaic populations and modern human populations, we assign the Xiahe mandible to a hominin population closely related to, or part of, the hominin population represented by the Denisovans from Denisova Cave (here represented by individual D3).

SI Table 5. Uniprot accession numbers for protein sequences of extant primates used in the phylogenetic analyses.

Gene	*Macaca mulatta*	*Nomascus leucogenys*	*Pongo abelii*	*Gorilla gorilla*	*Pan troglodytes*	*Homo sapiens*
COL10α1	G7MQP5	G1RRM5	H2PK45	G3S3J2	H2QTL5	COAA1
COL1α1	H9Z595	G1RCL9	H2NVM9	G3RBN8	H2QDE6	CO1A1
COL1α2	H9Z2D1	G1RZZ2	H2PMW7	G3QT97	H2QUY2	CO1A2
COL2α1	F7B3R3	G1S8A3	H2NH33	G3QNV9	H2R193	CO2A1
COL3α1	H2YUF2	G1R429	H2P837	G3RK87	H2QJ46	CO3A1
COL5α1	F7GXV4	(*absent*)	(*absent*)	G3R760	K7CMZ9	CO5A1
COL5α2	F6V6S9	G1R465	H2P838	G3RDT1	H2R6B8	CO5A2

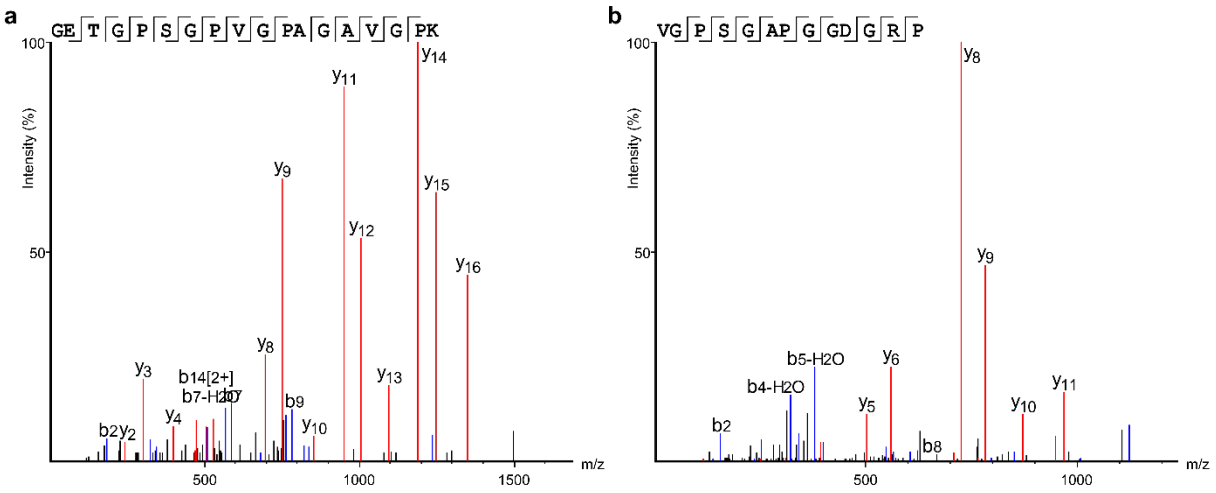

SI Figure 4. Examples of phylogenetically informative ancient peptide spectra from the Xiahe dentine extraction. a) *COL1α2*, positions 979 to 996. **b)** *COL2α1*, positions 575 to 587.

SUPPLEMENTARY REFERENCES

67. Arambourg, C. & Biberson, P. The fossil human remains from the Paleolithic site of Sidi Abderrahman (Morocco). *Am. J. Phys. Anthropol.* **14**, 467–489 (1956).
68. Sausse, F. La mandibule atlanthropienne de la Carriere Thomas I (Casablanca). *Anthropologie* **79**, 81–112 (1975).
69. Stewart, T. D. The skull of Shanidar II. *Annu. Rep. Board Regents Smithson. Inst.* 521–533 (1962).
70. Tillier, A.-M. La mandibule et les dents. *Le Squelette Moustérien de Kébara 2* 97–111 (1991).
71. Stewart, T. D. The Neanderthal skeletal remains from Shanidar Cave, Iraq: a summary of findings to date. *Proc. Am. Philos. Soc.* **121**, 121–165 (1977).
72. Trinkaus, E. *The Shanidar Neanderthals*. (Academic Press, 1983).
73. Leroi-Gourhan, A. *Etude des restes humains fossiles provenant des grottes d'Arcy-sur-Cure*. (Masson et Cie. éditeurs, 1958).
74. Topinard, P. *Les caracteres simiens de la machoire de la Naulette*. (1886).
75. Leguebe, A. & Toussaint, M. *La mandibule et les cubitus de la Naulette: morphologie et morphométrie*. (Editions du Centre national de la recherche scientifique, 1988).
76. Drozdová, E. A rediscovered fragment of a human mandible from Predmostí u Prerova (Czech Republic): Predmostí 21. *Bulletins et mémoires de la Société d'Anthropologie de Paris, 14 (1-2)* | *2002 2002(1-2)* (2002).
77. de Lumley, M.-A. Les Neandertaliens de la Grotte de l'Hortus. *Etudes Quaternaires (University de Province). Memoire* **1**, 375–385 (1972).
78. Condemi, S. *et al.* Possible interbreeding in late Italian Neanderthals? New data from the Mezzena jaw (Monti Lessini, Verona, Italy). *PLoS One* **8**, e59781 (2013).
79. Walker, M. J., Lombardi, A. V., Zapata, J. & Trinkaus, E. Neandertal mandibles from the Sima de las Palomas del Cabezo Gordo, Murcia, southeastern Spain. *Am. J. Phys. Anthropol.* **142**, 261–272 (2010).
80. Martin, H. Machoire humaine mousterienne: trouvee dans la station de la Quina. *L'Homme Prehistorique* **13**, 3–12 (1926).
81. Martin, H. Position stratigraphique des Ossements humains recueillis dans le Moustérien de La Quina de 1908 à 1912. *Bulletin de la Société préhistorique de France* **9**, 700–709 (1912).
82. Pap, I. The Subalyuk Neanderthal remains (Hungary): a re-examination. *Ann. Hist.-Nat. Mus. Natl. Hung.* **88**, 233–270 (1996).
83. Sanchez, F. Comparative biometrical study of the Mousterian mandible from Cueva del Boquete de Zafarraya (Málaga, Spain). *Hum. Evol.* **14**, 125–138 (1999).
84. Vlček, E. Fossile Menschenfunde von Weimar-Ehringsdorf. (1993).
85. Condemi, S. *Les néandertaliens de La Chaise: abri Bourgeois-Delaunay*. **15**, (Comité des travaux historiques et scientifiques-CTHS, 2001).
86. Arambourg, C. & Hoffstetter, R. *Le gisement de Ternifine*. **32**, (Masson, 1963).
87. Vallois, H. V. La mandibule humaine fossile de la Grotte du Porc-Epic près Diré-Daoua (Abyssinie). *Anthropologie* (1951).
88. Snow, C. E. *The ancient Palestinian: Skhul V reconstruction*. (Hugh Hencken, 1953).
89. Rightmire, G. P. & Deacon, H. J. Comparative studies of Late Pleistocene human remains from Klasies River Mouth, South Africa. *J. Hum. Evol.* **20**, 131–156 (1991).

90. Sollas, W. J. The Chancelade Skull. *The Journal of the Royal Anthropological Institute of Great Britain and Ireland* **57**, 89–122 (1927).
91. Henri-Martin, L. Caractères des squelettes humains quaternaires de la vallée du Roc (Charente). *Bull. Mem. Soc. Anthropol. Paris* **8**, 103–129 (1927).
92. Vercellotti, G., Alciati, G., Richards, M. P. & Formicola, V. The Late Upper Paleolithic skeleton Villabruna 1 (Italy): a source of data on biology and behavior of a 14,000 year-old hunter. *J. Anthropol. Sci.* **86**, 143–163 (2008).
93. Formicola, V. Una mandibola umana dal deposito dell'Epigravettiano finale delle Arene Candide (scavi 1970). *Rivista di antropologia* **64**, 271–278 (1986).
94. Odano, A. M. & Riquet, R. Le gisement préhistorique de Dar-es-Soltane 2. Champ de tir de El Menzeh à Rabat (Maroc). Note préliminaire. 2-Étude anthropologique des restes post-atériens. *Bull. d'Archéologie Marocaine* **11**, 25–63 (1978).
95. Debénath, A. Nouveaux restes humains atériens du Maroc. *CR Acad. Sci. Paris* **290**, 851–852 (1980).
96. Crognier, E. & Dupouy-Madre, M. Les Natoufiens du Nahal Oren (Ouadi Fallah): Etude Antrhopologique. *Paléorient* **2**, 103–121 (1974).
97. Henke, W. Vergleichend-morphologische Kennzeichnung der Jungpaläolithiker von Oberkassel bei Bonn. *Z. Morphol. Anthropol.* **75**, 27–44 (1984).
98. Hershkovitz, I. *et al.* Ohalo II H2: A 19,000-year-old skeleton from a water-logged site at the Sea of Galilee, Israel. *Am. J. Phys. Anthropol.* **96**, 215–234 (1995).
99. Soficaru, A., Doboş, A. & Trinkaus, E. Early modern humans from the Peştera Muierii, Baia de Fier, Romania. *Proc. Natl. Acad. Sci. U. S. A.* **103**, 17196–17201 (2006).
100. Crevecoeur, I. Etude anthropologique des restes humains de Nazlet Khater (Paléolithique supérieur, Egypte). (Université Sciences et Technologies-Bordeaux I, 2006).
101. Thoma, A. Morphology and affinities of the Nazlet Khater man. *J. Hum. Evol.* **13**, 287–296 (1984).
102. Anderson, J. E. Late Paleolithic skeletal remains from Nubia. *The prehistory of Nubia* **2**, 996–1040 (1968).
103. Crevecoeur, I. & Trinkaus, E. From the Nile to the Danube: a comparison of the Nazlet Khater 2 and Oase 1 early modern human mandibles. *Anthropologie* **42**, 203–214 (2004).
104. Trinkaus, E. *et al.* An early modern human from the Peştera cu Oase, Romania. *Proc. Natl. Acad. Sci. U. S. A.* **100**, 11231–11236 (2003).
105. Trinkaus, E. & Svoboda, J. *Early Modern Human Evolution in Central Europe: The People of Dolní Věstonice and Pavlov*. (Oxford University Press, 2006).
106. Sladek, V., Trinkaus, E., Hillson, S. W. & Holliday, T. W. *The people of the Pavlovian. Skeletal catalogue and osteometrics of the Gravettian fossil hominids from Dolni Vestonice and Pavlov*. 1–244 (Dolni Vestonice Studie, Svazek 5., 2000).
107. Dutour, O. Palimpseste paléoanthropologique sur l'Homme fossile d'Asselar (Sahara). *Préhistoire anthropologie méditerranéennes* **1**, 73–83 (1992).
108. Gambier, D. Les vestiges humains du gisement d'Isturitz (Pyrénées-Atlantiques). Étude anthropologique et analyse des traces d'action humaine intentionnelle. *Antiquités nationales* 9–26 (1990).
109. Billy, G. La mandibule pré-rissienne de Montmaurin. *Anthropologie* **81**, 411–458 (1977).

110. Wu, R. & Dong, X. Preliminary study of Homo erectus remains from Hexian, Anhui. *Acta Anthropologica Sinica* **1**, 2–13 (1982).
111. Weidenreich, F. The mandibles of Sinanthropus pekinensis: a comparative study. *Paleontologia Sinica, Ser. D* **7**, 1–162 (1936).
112. Tyler, D. E. Two new 'Meganthropus' mandibles from Java. *Hum. Evol.* **16**, 151–158 (2001).
113. Kaifu, Y., Aziz, F. & Baba, H. Hominid mandibular remains from Sangiran: 1952--1986 collection. *American Journal of Physical Anthropology* **128**, 497–519 (2005).
114. Weidenreich, F. Giant early man from Java and South China. *Science* **99**, 479–482 (1944).
115. Woo, J. K. & Chao, T. K. New discovery of Sinanthropus mandible from Choukoutien. *Vertebrata PalAsiatica* **3**, 169–172 (1959).
116. Matsumura, H. & Pookajorn, S. A morphometric analysis of the Late Pleistocene Human Skeleton from the Moh Khiew Cave in Thailand. *Homo* **56**, 93–118 (2005).
117. Martin, R. & Saller, K. Lehrbuch der Anthropologie. *Ⅱ: Gustav Fischer Verlag, Stuttgart* 775–786 (1959).
118. Trinkaus, E., Buzhilova, A. P., Mednikova, M. B. & Dobrovolskaya, M. V. *The People of Sunghir: Burials, Bodies, and Behavior in the Earlier Upper Paleolithic*. (Oxford University Press, 2014).
119. Buzi, C. *et al.* Measuring the shape: performance evaluation of a photogrammetry improvement applied to the Neanderthal skull Saccopastore 1. *ACTA IMEKO* **7**, 79–85 (2018).
120. Katz, D. & Friess, M. 3D from standard digital photography of human crania—a preliminary assessment. *Am. J. Phys. Anthropol.* **154**, 152–158 (2014).
121. Jurda, M. & Urbanová, P. Three-dimensional documentation of Dolní Věstonice skeletal remains: can photogrammetry substitute laser scanning? *Anthropologie* **54**, 109–118 (2016).
122. Arriaza, M. C. *et al.* On applications of micro-photogrammetry and geometric morphometrics to studies of tooth mark morphology: The modern Olduvai Carnivore Site (Tanzania). *Palaeogeogr. Palaeoclimatol. Palaeoecol.* **488**, 103–112 (2017).
123. Yravedra, J. *et al.* The use of Micro-Photogrammetry and Geometric Morphometrics for identifying carnivore agency in bone assemblages. *Journal of Archaeological Science: Reports* **14**, 106–115 (2017).
124. Porter, S. T., Roussel, M. & Soressi, M. A simple photogrammetry rig for the reliable creation of 3D artifact models in the field: lithic examples from the Early Upper Paleolithic sequence of Les Cottés (France). *Advances in Archaeological Practice* **4**, 71–86 (2016).
125. Knyaz, V. A., Leybova, N. A., Galeev, R., Novikov, M. & Gaboutchian, A. V. Photogrammetric techniques for paleoanthropological objects preserving and studying. *ISPRS - International Archives of the Photogrammetry, Remote Sensing and Spatial Information Sciences* **422**, 525–530 (2018).
126. Bräuer, G. & Mehlman, M. J. Hominid molars from a Middle Stone Age level at the Mumba Rock Shelter, Tanzania. *Am. J. Phys. Anthropol.* **75**, 69–76 (1988).
127. Protsch, R. R. R. Die Archäologischen und Anthropologischen Ergebnisse der Kohl-Larsen-Expeditionenin Nord-Tanzania 1933--1939. in *The Palaeoanthropological finds of the Pliocene and Pleistocene* 34 (Archeologica Venatoria Tübingen, 1981).
128. Wood, B. A. & Van Noten, F. L. Preliminary observations on the BK 8518 mandible from Baringo, Kenya. *Am. J. Phys. Anthropol.* **69**, 117–127 (1986).

129. Rightmire, G. P. Middle Pleistocene hominids from Olduvai Gorge, northern Tanzania. *Am. J. Phys. Anthropol.* **53**, 225–241 (1980).
130. Bermúdez de Castro, J. M. Dental remains from Atapuerca (Spain) I. Metrics. *J. Hum. Evol.* **15**, 265–287 (1986).
131. Grine, E. F. Fossil hominid teeth from the Sangiran Dome (Java, Indonesia). *Cour. Forschungsinst. Senckenb.* **171**, 75–103 (1994).
132. Zanolli, C. Additional evidence for morpho-dimensional tooth crown variation in a New Indonesian H. erectus sample from the Sangiran Dome (Central Java). *PLoS One* **8**, e67233 (2013).
133. Bailey, S. E. Neandertal dental morphology: implications for modern human origins. (Arizona State University Tempe, 2002).
134. Fabbri, P. F. Dental anthropology of the Upper Palaeolithic sample from San Teodoro and inference on the peopling of Sicily. *Z. Morphol. Anthropol.* **80**, 311–327 (1995).
135. Ferraz, J. A. & Pécora, J. D. Three-rooted mandibular molars in patients of Mongolian, Caucasian and Negro origin. *Braz. Dent. J.* **3**, 113–117 (1993).
136. Tu, M.-G. *et al.* Detection of permanent three-rooted mandibular first molars by cone-beam computed tomography imaging in Taiwanese individuals. *J. Endod.* **35**, 503–507 (2009).
137. Turner, C. G. Three-rooted mandibular first permanent molars and the question of American Indian origins. *Am. J. Phys. Anthropol.* **34**, 229–241 (1971).
138. Molnar, S. Human tooth wear, tooth function and cultural variability. *Am. J. Phys. Anthropol.* **34**, 175–189 (1971).
139. 1000 Genomes Project Consortium *et al.* A global reference for human genetic variation. *Nature* **526**, 68–74 (2015).
140. Lek, M. *et al.* Analysis of protein-coding genetic variation in 60,706 humans. *Nature* **536**, 285–291 (2016).